

# Development of a Monitoring System for Semicontinuous Measurements of Stable Carbon Isotope Ratios in Atmospheric Carbonaceous Aerosols: Optimized Methods and Application to Field Measurements

Yu-Chi Lin, Yan-Lin Zhang,\* Feng Xie, Wen-Qi Zhang, Mei-Yi Fan, Zhiwei Lin, Chris W. Rella, and John A. Hoffnagle



Cite This: <https://dx.doi.org/10.1021/acs.analchem.0c02063>



Read Online

ACCESS |



Metrics & More

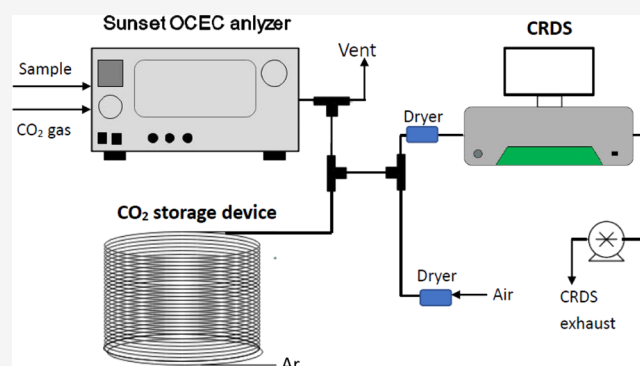


Article Recommendations



Supporting Information

**ABSTRACT:** Carbon content constitutes a major fraction of atmospheric particulate matter (PM) and directly influences the earth's climate and human health. The stable carbon isotope ratios ( $\delta^{13}\text{C}$ ) can be used to track potential sources and atmospheric processes of carbonaceous aerosols. Previously, determination of  $\delta^{13}\text{C}$  was always conducted in offline carbonaceous aerosol samples. The poor time-resolution results cannot provide information regarding the temporal evolution of  $\delta^{13}\text{C}$  at a short-time scale. In this study, we developed a new system for online measurements of  $\delta^{13}\text{C}$  in atmospheric carbonaceous aerosols by combining a semicontinuous organic carbon/elemental carbon (OC/EC) analyzer and online cavity ring-down spectroscopy (CRDS) (OC/EC analyzer-CRDS). To provide better stability in the determination of  $\delta^{13}\text{C}$ , a carrier gas with  $\text{CO}_2$  ( $\sim 200$  ppm) in "balance gas" was used, and Keeling analysis was employed to separate the  $\delta^{13}\text{C}$  signal of the sample from background  $\text{CO}_2$  gas. Our results showed that the accuracy and absolute precision of the  $\delta^{13}\text{C}$  measurements by the OC/EC analyzer-CRDS system were better than  $0.1\text{‰}$  and  $0.5\text{‰}$ , respectively, for the samples containing carbon content more than  $5 \mu\text{g}$ . Furthermore, we employed this system to monitor  $\delta^{13}\text{C}$  ( $\delta^{13}\text{C}$ -TC) in particulate total carbon (TC) with a time resolution of 2–4 h over Beijing in late summer and early autumn, 2019. During the sampling period, the TC concentrations varied from  $0.1$  to  $12.0 \mu\text{g m}^{-3}$  with a mean value of  $6.0 \pm 2.4 \mu\text{g m}^{-3}$ . The  $\delta^{13}\text{C}$ -TC ranged from  $-28.2$  to  $-24.2\text{‰}$  (mean value was  $-25.9 \pm 0.9\text{‰}$ ) without significant diurnal variations, suggesting similar contributing sources to TC. Comparing the  $\delta^{13}\text{C}$  signatures of different emissions, we found that liquid fuels and primary and secondary  $\text{C}_3$  plants were likely the dominant sources of particulate TC. Finally, we found that atmospheric heavy precipitation washed out the aged aerosols from the polluted air, resulting in significant depletion ( $\sim 2.4\text{‰}$ ) of  $\delta^{13}\text{C}$ -TC in the atmosphere. This paper described a novel system for conducting online measurements of  $\delta^{13}\text{C}$  in atmospheric carbonaceous aerosols and provided us information to better understand the temporal evolution of emission sources and atmospheric processes of carbonaceous aerosols.



## 1. INTRODUCTION

Carbonaceous aerosols contribute a major fraction (20–50%) of atmospheric fine particulate matter ( $\text{PM}_{2.5}$ , with an aerodynamic diameter of less than  $2.5 \mu\text{m}$ ) in the urban polluted atmosphere.<sup>1–3</sup> Total carbon (TC) aerosols are composed mainly of a complex mixture of carbon atoms and can be classified into two major fractions: one is organic carbon (OC) and another is elemental carbon (EC). OC is mainly emitted from both primary sources and secondary transformation from volatile organic compounds (VOCs), while EC is profoundly emitted from incomplete combustion processes, such as vehicle emission, industrial processing, biomass burning (BB), and coal combustion.<sup>4</sup> In addition to health risk effects, carbonaceous aerosols exert potentially

warming and cooling effects on the Earth system, resulting in changes in cloud formation, precipitation, and Earth's climate.<sup>5–7</sup> Thus, carbonaceous aerosols have been receiving more attention in the past decades.

Tracking potential sources of carbonaceous aerosols gives important information for policy makers to formulate strategies to improve the air quality and decrease health risks in the

Received: May 13, 2020

Accepted: September 25, 2020

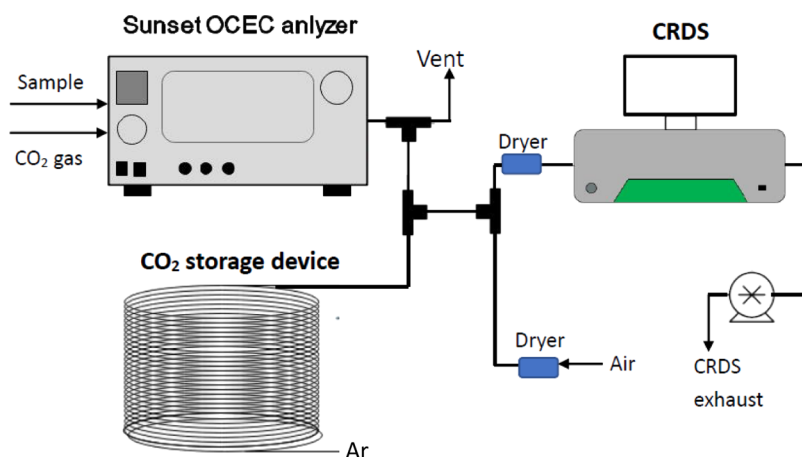


**Figure 1.** Schematic diagram of the OC/EC analyzer-CRDS system developed in this study.

polluted atmosphere. Over the last decades, several approaches, including the chemical mass balance model, positive matrix factorization (PMF), macrotracer method, and stable and radiocarbon isotope techniques, have been employed to identify potential sources of atmospheric carbonaceous aerosols.<sup>8–12</sup> Among these methods, the stable carbon isotope technique is a useful tool to track sources for particulate carbon and is advantageous from the point of view that it does not require many samples and extended data sets.<sup>13,14</sup> Because of isotope fractionation, stable carbon isotope values ( $\delta^{13}\text{C}$ ) in different emission sources have their own unique signatures. Previous studies have shown that  $\delta^{13}\text{C}$  of aerosols from combustion of liquid fuels, including gasoline, diesel, natural gas, and fuel oil, varied from  $-28.0$  to  $-24.0\text{‰}$ ,<sup>15–17</sup> which was more depleted than those derived from coal combustion ( $-25.0$  to  $-21.0\text{‰}$ ).<sup>15,18</sup> BB has a large contribution to atmospheric carbonaceous aerosols. Burning of  $\text{C}_3$  and  $\text{C}_4$  plants releases carbonaceous aerosols into the atmosphere with different  $\delta^{13}\text{C}$  features. Compared to  $\text{C}_3$  plants ( $\delta^{13}\text{C}$ :  $-34.7$  to  $-23.0\text{‰}$ ), burning of  $\text{C}_4$  plants produces carbonaceous aerosols with enriched  $\delta^{13}\text{C}$  values, which was from  $-19.9$  to  $-11.1\text{‰}$ .<sup>19–22</sup> Using isotope techniques, numerous studies have successfully tracked and quantified potential sources of atmospheric carbonaceous aerosols over the last decade.<sup>18,23–27</sup> Utilizing  $\delta^{13}\text{C}$  techniques, Cao et al.<sup>18</sup> found that  $\text{PM}_{2.5}$  carbon in China was dominated from traffic emission and coal combustion; in particular, coal combustion contributed significantly to carbonaceous aerosols in northern China during wintertime. Zhao et al.<sup>26</sup> performed source apportionments of EC particles in Xi'an in northwest China. They concluded that vehicle emission and coal combustion were major sources of airborne EC in Xi'an. Both sources contributed approximately 46% to particulate EC on a yearly basis. In addition,  $\delta^{13}\text{C}$  can also be used to track atmospheric processes, such as secondary formation and photochemical aging process of carbonaceous aerosols.<sup>14,24,28</sup> In general, heavier  $\delta^{13}\text{C}$  was observed in aged aerosols because of the addition of more oxygenated function groups by photochemical oxidation/aging processes during their long-range transport.<sup>14,28–30</sup>

To obtain  $\delta^{13}\text{C}$  values in ambient particles, offline collected carbon aerosol samples (sampling duration was regularly 12 h or 24 h) must be converted to  $\text{CO}_2$  through the combustion process; the carbon isotopes of the produced  $\text{CO}_2$  are then determined by isotope ratio mass spectroscopy (IRMS).<sup>18,29,31</sup>

The isotopic composition in the low time-resolution aerosol samples cannot provide insights to understand the temporal evolution of  $\delta^{13}\text{C}$  associated with some atmospheric processes which usually occur on an hourly scale.<sup>14</sup> Recently, a spectroscopic technique (cavity ring-down spectroscopy, CRDS) has been developed to measure carbon isotopes in ambient  $\text{CO}_2$ . Compared to IRMS, CRDS exhibits relatively poor accuracy and precision ( $0.2\text{‰}$  for 2 min average)<sup>32</sup> for analyzing carbon isotopes. Nevertheless, it provides data with high temporal resolution (1 Hz); therefore, this spectroscopic technique was appropriate to use for continuously monitoring carbon isotopes of  $\text{CO}_2$  in ambient levels.<sup>32</sup> This function is very important and provides us a hint for better understanding the temporal evolution of atmospheric processes in carbonaceous aerosols. For OC/EC observation, a Sunset OC/EC analyzer is an instrument which enables quantifying carbon content by concentration determination of  $\text{CO}_2$  obtained from the oxidation of carbonaceous aerosols based on the thermal desorption method. This instrument has been widely employed to measure carbon concentrations in atmospheric aerosols with a time resolution of 1 h.<sup>33,34</sup>

In this work, we developed a new system, in which a Sunset OC/EC analyzer was connected to a CRDS (OC/EC analyzer-CRDS hereafter) system, in order to synchronously conduct online measurements of mass concentrations and carbon isotopic compositions of ambient carbonaceous aerosols. We validated the performance of OC/EC analyzer-CRDS in measurement of  $\delta^{13}\text{C}$  by comparing the results with a traditional IRMS. Finally, we employed this system to continuously monitor the concentrations and  $\delta^{13}\text{C}$  in particulate TC in Beijing. Based on the high time-resolution data, we explored the potential sources and atmospheric processes contributing to the atmospheric carbonaceous aerosols in the capital city of China.

## 2. EXPERIMENT

### 2.1. Setup of the OC/EC Analyzer-CRDS System.

In this study, we connected a Sunset OC/EC analyzer with a CRDS system for continuously monitoring carbon isotopic compositions in carbonaceous aerosols and validated the performance of this system. Figure 1 shows the schematic diagram of the OC/EC analyzer-CRDS system. In brief, this system consisted mainly of three parts, including an OC/EC analyzer (model 3F, Sunset Laboratory Inc., Portland, OR, USA), a  $\text{CO}_2$  storage device (consisted mainly of aluminum

pipe without any coating, and I.D. of the pipe was 0.315 inches), and a CRDS system (G2201-i, Picarro, Santa Clara, USA). During sampling, the ambient air was pulled in with a flow rate of 8 L min<sup>-1</sup> for 45 min (for 1 h time resolution sampling) through a cyclone to remove particles larger than 2.5 μm, leaving other particulate aerosols deposited on a quartz filter inside the OC/EC analyzer. After filtration, the collected aerosols underwent the combustion process (duration time was 15 min, and flow rate was 70 mL min<sup>-1</sup>), followed by a pulse of methane of a known concentration (CH<sub>4</sub>, for quantification of carbon content in aerosols), in the oven under a mixed atmospheric (90% Ar + 10% O<sub>2</sub> + ~200 ppm CO<sub>2</sub>) condition. The combusted carbonaceous aerosols along with CH<sub>4</sub> were then converted to CO<sub>2</sub> by a redox reaction with manganese dioxide (MnO<sub>2</sub>). The total concentration of the newly generated CO<sub>2</sub> and the background CO<sub>2</sub> (~200 ppm) from the cylinder was quantified by nondispersive infrared absorption (NDIR) inside the OC/EC analyzer. This background CO<sub>2</sub> provided here was used to improve the signal and stability of carbon isotope values determined in CRDS afterward (this will be discussed in Section 3.1). Subsequently, the produced CO<sub>2</sub> gas pulses measured by NDIR were injected into the CO<sub>2</sub> storage device. The stored CO<sub>2</sub> gas pulses were then introduced into the CRDS system in reverse flow with a rate of 10 mL min<sup>-1</sup> (duration time was about 42 min). At the same time, the OC/EC analyzer started the next aerosol sampling cycle followed by the combustion process. Water vapor in air samples would result in slight effects on measured δ<sup>13</sup>C values by CRDS,<sup>32</sup> and therefore, water vapor must be removed from air samples by the dryers filled with magnesium perchlorate (Mg(ClO<sub>4</sub>)<sub>2</sub>) before entering into the CRDS system.

The δ<sup>13</sup>C of the produced CO<sub>2</sub> was determined by CRDS, which is a high-sensitivity laser absorption technique to monitor the mass concentrations and carbon isotopes in trace gases, of course, including CO<sub>2</sub> under ambient-level conditions.<sup>32</sup> Besides, CRDS also has a well-designed pressure and temperature control system to ensure high stability of these measurements. The details of CRDS can be found elsewhere.<sup>35</sup> In this study, the produced CO<sub>2</sub> was constantly pulled into a high-reflectivity cell with a volume of 35 cm<sup>3</sup>, operated at an inlet flow rate of 10 mL min<sup>-1</sup>. The temperature and pressure inside the cell were maintained at 318.15 K and 18.7 kPa, respectively. The abundances of <sup>12</sup>C–CO<sub>2</sub> and <sup>13</sup>C–CO<sub>2</sub> were then independently measured at wavelengths near 6251 cm<sup>-1</sup>, and δ<sup>13</sup>C can be then calculated following the equation

$$\delta^{13}\text{C}(\text{‰}) = \left[ \left( \frac{{}^{13}\text{C}/{}^{12}\text{C}}{\text{sample}} \right) / \left( \frac{{}^{13}\text{C}/{}^{12}\text{C}}{\text{VPDB}} \right) - 1 \right] \times 1000 \quad (1)$$

where (<sup>13</sup>C/<sup>12</sup>C)<sub>sample</sub> is the <sup>13</sup>C/<sup>12</sup>C ratio of the produced CO<sub>2</sub> in samples and (<sup>13</sup>C/<sup>12</sup>C)<sub>VPDB</sub> is the isotope ratio of Vienna Pee Dee Belemnite (VPDB).

**2.2. Output of the OC/EC Analyzer.** Figure S1a shows the output of heating temperature and CO<sub>2</sub> signals using the OC/EC analyzer at a time resolution of 1 Hz. During the combustion process, the oven inside the OC/EC analyzer was heated from 70 to 850 °C within 2 min, remaining at this temperature for 2.5 min and then decreasing to 70 °C within 1.5 min. Subsequently, the instrument was flushed with Ar for 2 min and then switched to the standby mode automatically for nearly 7 min. Under this heating condition, the CO<sub>2</sub> signals produced by carbonaceous aerosols were found between 0.67

and 2.67 min and that converted from CH<sub>4</sub> was found between 4.4 and 5.4 min. The concentrations of CO<sub>2</sub> from carbonaceous aerosols and methane were automatically obtained by subtracting the concentrations of total CO<sub>2</sub> (sample + background) from the background gas; the carbon content (μg) can be calculated from the peak areas of CO<sub>2</sub> produced by carbonaceous aerosols with the correlation between the peak area and the carbon content determined from the CH<sub>4</sub> with a known amount.

A Sunset OC/EC analyzer has been widely used to continuously monitor OC and EC concentrations in atmospheric aerosols.<sup>33</sup> In each run, in situ analysis of OC and EC in aerosols was conducted by the NIOSH 5040 thermal–optical protocol (Table S1 and Supporting Information S1) after an aerosol sample was collected.<sup>36</sup> In the NIOSH 5040 protocol, the concentrations of TC were, in general, calculated by the sum of the concentrations of OC and EC. In this work, we directly measured TC concentration by heating the aerosol samples from 70 to 850 °C under a mixed atmospheric (90% Ar + 10% O<sub>2</sub> + ~200 ppm CO<sub>2</sub>) condition. Because of the significant different combustion procedures between our method and the NIOSH 5040, the comparisons of TC concentrations measured by the two different heating procedures were needed. To achieve this goal, a total of seven 24 h PM<sub>2.5</sub> aerosol samples were collected on the campus of Nanjing University of Information Science and Technology (NUIST) using a high-volume PM<sub>2.5</sub> sampler (Tisch-PM<sub>2.5</sub>, USA), operated at a flow rate of 1.13 m<sup>3</sup> min<sup>-1</sup>, from 2019 March 5 to 11. The preheated (450 °C for 6 h) 8 × 10 in. quartz filter membranes (TISSUQUARTZ-2500QAT-UP, PALL, USA) were used as substrates to collect the PM<sub>2.5</sub> samples. After sampling, two pieces of the 0.625 cm<sup>2</sup>-punched quartz filter (varied from 10 to 40 μgC) were used to individually analyze the concentrations of TC through our heating procedure and measure OC and EC concentrations by the NIOSH 5040. The TC concentrations measured by the NIOSH 5040 were then calculated by the sum of OC and EC.<sup>33,36</sup> Figure S2 shows the TC concentrations measured by the two different procedures. As can be seen, a good correlation (the coefficient of determination, R<sup>2</sup>, was 0.99 with a 95% significance confidence interval, *p* < 0.05) of TC concentrations was found between the two different heating procedures with a slope of 0.97. This indicated that TC concentrations analyzed in our heating procedure were reliable.

**2.3. Stability of CRDS.** After combustion, the produced CO<sub>2</sub> entered into the CO<sub>2</sub> storage device with a volume of 420 mL (70 mL min<sup>-1</sup> × 6 min). Subsequently, the produced CO<sub>2</sub> was sent to the CRDS system with a flow rate of 10 mL min<sup>-1</sup>. This indicated that the analysis time of δ<sup>13</sup>C in the produced CO<sub>2</sub> by CRDS was 42 min. After that, the ambient air was introduced into the CRDS system and analyzed for carbon isotopic compositions for another 18 min. However, the δ<sup>13</sup>C values of the ambient samples were not used to inspect the stability of the CRDS system. Figure S1b plots the output of CO<sub>2</sub> signals and δ<sup>13</sup>C values measured by CRDS at a frequency of 1 Hz. The CO<sub>2</sub> signals shown here are the sum of background CO<sub>2</sub> (~200 ppm) and that produced by CH<sub>4</sub>/carbonaceous aerosols; therefore, the CO<sub>2</sub> concentrations detected by CRDS were, in general, 200 ppm higher than those detected using the OC/EC analyzer. Note that the order of the appearance in peaks of CH<sub>4</sub> and carbonaceous aerosols was opposite to that measured using the OC/EC analyzer because CO<sub>2</sub> produced from CH<sub>4</sub> was introduced into the CRDS

system from the storage device before the CO<sub>2</sub> from carbonaceous aerosols because of the reverse flow.

Stability of CRDS was checked by the long-term variability of  $\delta^{13}\text{C}$  values measured from 200 ppm background CO<sub>2</sub> gas. Figure S3 shows the  $\delta^{13}\text{C}$  values (2 min average) of the background CO<sub>2</sub> gas during the Beijing campaign. The result indicated that the  $\delta^{13}\text{C}$  values determined by CRDS were likely normally distributed. The long-term ( $N = 588$ ) absolute precision of the 2 min-averaged value was about 0.26‰, indicating slight drifts during the 20 day sampling period. The absolute precision was also in agreement with that by Vogel et al.<sup>32</sup> who suggested that the precision of  $\delta^{13}\text{C}$  determined by CRDS was approximately 0.25‰ with the 2 min-averaged data.

### 3. RESULTS AND DISCUSSION

#### 3.1. Effect of CO<sub>2</sub> Concentrations on the $\delta^{13}\text{C}$ Values.

Furthermore, we tested the performance of the OC/EC analyzer-CRDS system in determination of  $\delta^{13}\text{C}$  by the three working standards. Previous studies have shown that the CRDS system had the capacity to make isotopic measurements of CO<sub>2</sub> in which the concentration was higher than approximately 300 ppm.<sup>32</sup> The requirement of 300 ppm CO<sub>2</sub> for CRDS was equal to 24  $\mu\text{gC}$  of carbon content (calculated from Table 1) without adding any background

**Table 1. Produced CO<sub>2</sub> Concentrations (Sample + Background) and Their Accompanying  $\delta^{13}\text{C}$  Values of Various Carbon Contents in the Three Working Standards**

working standards ( $\mu\text{g}$ )	CO <sub>2</sub> (ppm)	$\delta^{13}\text{C}$ (‰)	corrected- $\delta^{13}\text{C}$ (‰) <sup>a</sup>
KHP (-30.4‰)			
2.6 ± 0.2	246 ± 3	-12.63 ± 0.20	-17.47 ± 0.92
5.3 ± 0.1	290 ± 6	-13.07 ± 0.12	-16.43 ± 0.38
10.5 ± 0.3	359 ± 7	-13.93 ± 0.11	-16.95 ± 0.22
20.3 ± 0.6	448 ± 17	-14.34 ± 0.25	-16.58 ± 0.14
38.4 ± 3.3	690 ± 42	-15.19 ± 0.24	-16.68 ± 0.08
81.1 ± 2.7	984 ± 70	-15.83 ± 0.05	-16.94 ± 0.06
sucrose A (C <sub>3</sub> plants, -25.0‰)			
2.7 ± 0.3	245 ± 5	-11.10 ± 0.14	-6.15 ± 1.19
5.4 ± 0.3	284 ± 5	-11.16 ± 0.07	-10.37 ± 0.48
10.5 ± 0.4	350 ± 4	-11.21 ± 0.07	-10.23 ± 0.39
20.3 ± 0.7	480 ± 6	-11.18 ± 0.12	-10.65 ± 0.19
37.8 ± 3.0	696 ± 25	-11.06 ± 0.06	-10.72 ± 0.10
82.7 ± 4.8	1078 ± 65	-11.10 ± 0.07	-10.92 ± 0.07
sucrose B (C <sub>4</sub> plants, -12.2‰)			
3.0 ± 0.4	256 ± 3	-9.40 ± 0.25	2.23 ± 0.99
5.5 ± 0.2	292 ± 13	-8.13 ± 0.28	2.05 ± 0.39
9.6 ± 0.3	337 ± 11	-6.11 ± 0.29	2.21 ± 0.21
19.0 ± 0.6	478 ± 10	-3.64 ± 0.10	2.00 ± 0.12
41.3 ± 1.1	727 ± 7	-2.09 ± 0.16	1.92 ± 0.08
81.1 ± 2.7	1232 ± 10	-0.29 ± 0.06	2.11 ± 0.06

<sup>a</sup>The uncertainty of the corrected  $\delta^{13}\text{C}$  values was calculated by error propagation.

CO<sub>2</sub> gas in the system. The high required amount of carbon content ( $\sim 24 \mu\text{gC}$ ) was difficult for us to conduct online measurements of  $\delta^{13}\text{C}$  in aerosol samples with high-time resolution (2–4 h for one sample). To decrease the requirement of carbon content for  $\delta^{13}\text{C}$  measurements in carbonaceous aerosol samples, adding CO<sub>2</sub> as a background gas was needed. Here, we first tested the repeatability of  $\delta^{13}\text{C}$

measurements with/without adding CO<sub>2</sub> gases into the system. The various scenarios of different concentration (3, 5, 10, 20, 40, and 80  $\mu\text{gC}$ ) working standards [sucrose A from C<sub>3</sub> plants, sucrose B from C<sub>4</sub> plants, and potassium hydrogen phthalate (KHP)] mixed with different-level background CO<sub>2</sub> gases (0, 200, and 1000 ppm) were tested. This indicated that a total of 54 scenarios were made in the test. In each scenario, the working standard was placed in the oven inside the OC/EC analyzer for combustion, storage, and determination of <sup>12</sup>C–CO<sub>2</sub> and <sup>13</sup>C–CO<sub>2</sub> by CRDS, as mentioned in Section 2. The analysis of the  $\delta^{13}\text{C}$  value of each scenario was made with five repetitions ( $N = 5$ ). Figure 2 shows the standard deviation of  $\delta^{13}\text{C}$  values of the various carbon contents in KHP, sucrose A, and sucrose B mixed with the different-level (0, 200, and 1000 ppm) background CO<sub>2</sub> gases. The results showed that the large standard deviations of  $\delta^{13}\text{C}$  were found in all working standards without adding any background CO<sub>2</sub> gas, especially under the low carbon content conditions ( $< 3 \mu\text{gC}$ , the standard deviation was from 0.45 to 0.85‰). After adding the background CO<sub>2</sub> gases, the standard deviations of  $\delta^{13}\text{C}$  decreased significantly and were usually lower than 0.13‰ containing a carbon content of larger than 5  $\mu\text{gC}$ . This elucidated that increases in background CO<sub>2</sub> decreased the standard deviation of  $\delta^{13}\text{C}$ . In other words, adding background CO<sub>2</sub> gas in the system would improve the precision of  $\delta^{13}\text{C}$  measurement. In our test, the standard deviations of  $\delta^{13}\text{C}$  in the different carbon contents under 200 ppm- and 1000 ppm-CO<sub>2</sub> conditions were similar, and therefore, 200 ppm-level CO<sub>2</sub> was finally selected as the background gas for the measurements of  $\delta^{13}\text{C}$  for standards and atmospheric aerosols.

Next, we used the three different working standards mixed with background CO<sub>2</sub> gas ( $\sim 200$  ppm) to check the drifts of  $\delta^{13}\text{C}$  determined by this new system. Again, the measurement of  $\delta^{13}\text{C}$  values of each specific carbon content (approximately 3, 5, 10, 20, 40, and 80  $\mu\text{g}$ ) in each working standard was made with five repetitions ( $N = 5$ ). Figure S4 plots the drifts of  $\delta^{13}\text{C}$  values depending on various CO<sub>2</sub> concentrations (sample and background) produced by the three different working standards. The scatter plot of carbon contents versus produced CO<sub>2</sub> concentrations in the different standards (sample + background) is shown in Figure S5. As expected, the produced CO<sub>2</sub> concentrations were linearly correlated with carbon contents without any drifts. As shown in Figure S4, the  $\delta^{13}\text{C}$  values of KHP and sucrose B were significantly dependent on CO<sub>2</sub> concentrations, and the  $\delta^{13}\text{C}$  values depending on CO<sub>2</sub> concentrations measured by CRDS has been found in an earlier study.<sup>37</sup> For example, the measured  $\delta^{13}\text{C}$  value of KHP was about  $-12.6 \pm 0.2$ ‰ when the CO<sub>2</sub> concentration was  $246 \pm 32$  ppm (carbon content =  $2.6 \pm 0.2 \mu\text{g}$ , see in Table 1). When the CO<sub>2</sub> concentration increased to  $984 \pm 70$  ppm (carbon content =  $81.1 \pm 2.7 \mu\text{g}$ ), the  $\delta^{13}\text{C}$  value got depleted to  $-15.8 \pm 0.1$ ‰. Consequently, we had to develop the correction curve prior to online measurements of  $\delta^{13}\text{C}$  using a Keeling approach to estimate and to correct the real  $\delta^{13}\text{C}$  values generated by the standard,<sup>38</sup> and this will be discussed in the next section.

**3.2. Keeling Approach Results.** Three working standards of known  $\delta^{13}\text{C}$  values along with a known concentration of background CO<sub>2</sub> gas (200 ppm) were used to evaluate the performance of the OC/EC analyzer-CRDS system. Two challenges existed here. First, we had to decrease the dependence of  $\delta^{13}\text{C}$  varying with CO<sub>2</sub> concentrations (see in Figure S4) measured by this new system. Second, the

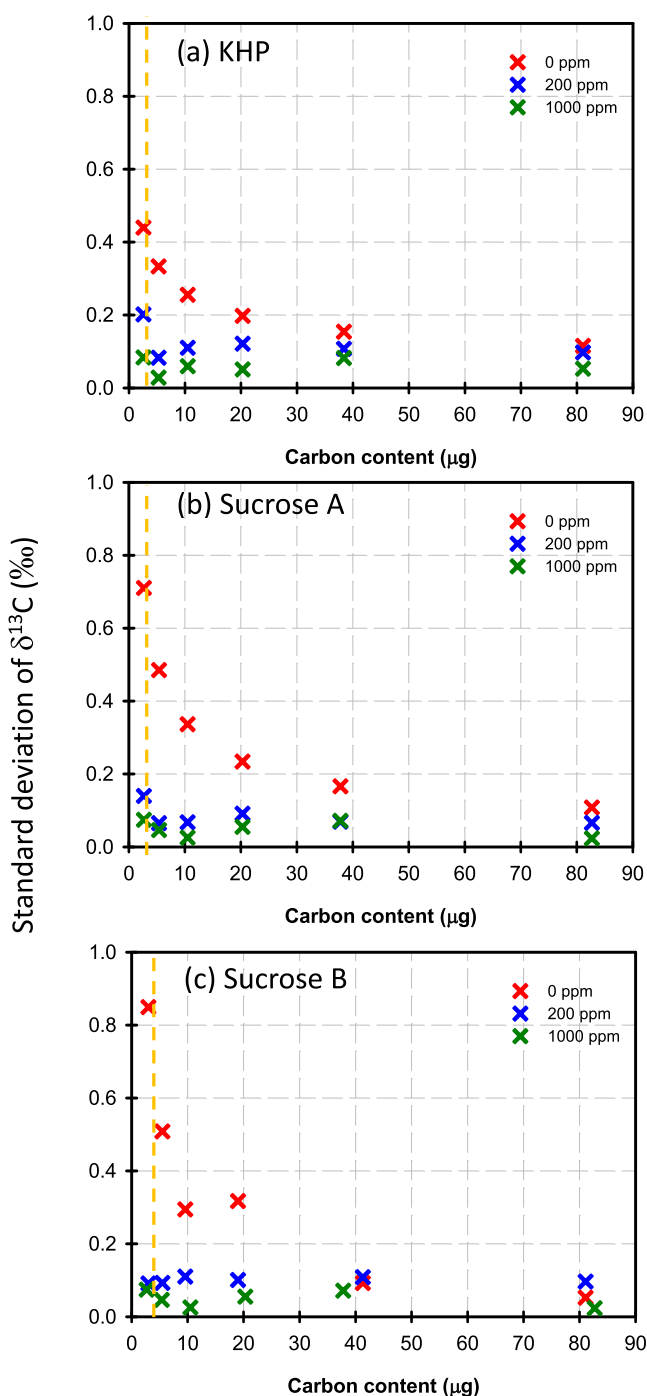


**Figure 2.** Standard deviations of  $\delta^{13}\text{C}$  values measured in (a) KHP, (b) sucrose A, and (c) sucrose B with different carbon contents. Five replicates of the same sample were measured to determine the standard deviation. The yellow dash lines denote a carbon content of 3  $\mu\text{gC}$ .

separation of  $\delta^{13}\text{C}$  values of sample  $\text{CO}_2$  (from standards) from the mixed  $\text{CO}_2$  (sample + background) was needed. To achieve this goal, the Keeling approach was subsequently used in the corrections.<sup>14,38–40</sup> Details of the Keeling approach can be found in Supporting Information S2. Figure S6 shows the scatter plot between  $\delta^{13}\text{C}_m$  ( $\delta^{13}\text{C}_m$  is the  $\delta^{13}\text{C}$  value of the mixed  $\text{CO}_2$  determined by CRDS) versus  $1/A_m$  ( $A_m$  is the peak area of mixed  $\text{CO}_2$  determined by CRDS) in the three working standards. The results showed good correlations ( $R^2 = 0.68–$

0.99) between  $\delta^{13}\text{C}_m$  and  $1/A_m$  for all the three working standards.

Based on the Keeling approach theory, linear regression of  $\delta^{13}\text{C}_m$  and  $1/A_m$  for any two standards (method I: KHP vs sucrose A, method II: KHP vs sucrose B, and method III: sucrose A vs sucrose B) can be used to calculate the corrected  $\delta^{13}\text{C}$  value ( $\delta^{13}\text{C}_{s\text{-corr}}$ ) of each working standard.<sup>14</sup> According to the Keeling approach (eq S4), the mixed  $\delta^{13}\text{C}$  values (produced by the standard and background) in the two standards determined by CRDS can be expressed as

$$\delta^{13}\text{C}_{m\text{-std1}} = \delta^{13}\text{C}_{s\text{-corr-std1}} + \frac{A_b(\delta^{13}\text{C}_b - \delta^{13}\text{C}_{s\text{-corr-std1}})}{A_{m\text{-std1}}} \quad (2)$$

$$\delta^{13}\text{C}_{m\text{-std2}} = \delta^{13}\text{C}_{s\text{-corr-std2}} + \frac{A_b(\delta^{13}\text{C}_b - \delta^{13}\text{C}_{s\text{-corr-std2}})}{A_{m\text{-std2}}} \quad (3)$$

where  $\delta^{13}\text{C}_{m\text{-std1}}$  and  $\delta^{13}\text{C}_{m\text{-std2}}$  are the mixed  $\delta^{13}\text{C}$  values in the different standards determined by CRDS and  $\delta^{13}\text{C}_b$  is the  $\delta^{13}\text{C}$  value of the background  $\text{CO}_2$  gas measured by CRDS.  $\delta^{13}\text{C}_{s\text{-corr-std1}}$  and  $\delta^{13}\text{C}_{s\text{-corr-std2}}$  are the corrected  $\delta^{13}\text{C}$  values of the different standards measured by CRDS.  $A_{m\text{-std1}}$  and  $A_{m\text{-std2}}$  are the mixed peak areas in the different standards, while  $A_b$  is the peak area in the background  $\text{CO}_2$  gas determined by CRDS. In eqs 2 and 3, the regression slopes of standards 1 ( $s_1$ ) and 2 ( $s_2$ ) can be expressed as

$$s_1 = A_b \times (\delta^{13}\text{C}_b - \delta^{13}\text{C}_{s\text{-corr-std1}}) \quad (4)$$

$$s_2 = A_b \times (\delta^{13}\text{C}_b - \delta^{13}\text{C}_{s\text{-corr-std2}}) \quad (5)$$

The regression intercepts of standards 1 and 2 can be expressed as

$$i_1 = \delta^{13}\text{C}_{s\text{-corr-std1}} \quad (6)$$

$$i_2 = \delta^{13}\text{C}_{s\text{-corr-std2}} \quad (7)$$

All the slopes ( $s_1$  and  $s_2$ ) and intercepts ( $i_1$  and  $i_2$ ) can be obtained by the linear regression between the mixed  $\delta^{13}\text{C}$  values and peak areas of the different working standards.

According to the eqs 4–7,  $A_b$  and  $\delta^{13}\text{C}_b$  can be expressed as

$$A_b = \frac{s_2 - s_1}{i_1 - i_2} \quad (8)$$

$$\delta^{13}\text{C}_b = \frac{s_2 \times i_1 - s_1 \times i_2}{s_2 - s_1} \quad (9)$$

Finally, the  $\delta^{13}\text{C}_{s\text{-corr}}$  of each standard can be calculated as

$$\delta^{13}\text{C}_{s\text{-corr}} = \frac{\delta^{13}\text{C}_m \times A_m - \delta^{13}\text{C}_b \times A_b}{A_m - A_b} \quad (10)$$

Figure 3 shows the corrected  $\delta^{13}\text{C}$  values depending on various  $\text{CO}_2$  (carbon content) concentrations in each working standard using the different methods. The scattered corrected  $\delta^{13}\text{C}$  values were detectable in all the working standards when the  $\text{CO}_2$  concentrations were less than 260 ppm (carbon content  $\sim 3 \mu\text{g} + 200 \text{ ppm}$  background  $\text{CO}_2$  gas). Nevertheless, the standard deviation of corrected  $\delta^{13}\text{C}$  decreased significantly, while the carbon contents increased. Compared to methods I and III, the average corrected  $\delta^{13}\text{C}$  values obtained by method II kept the constant levels in the different weights of carbon contents in individual working

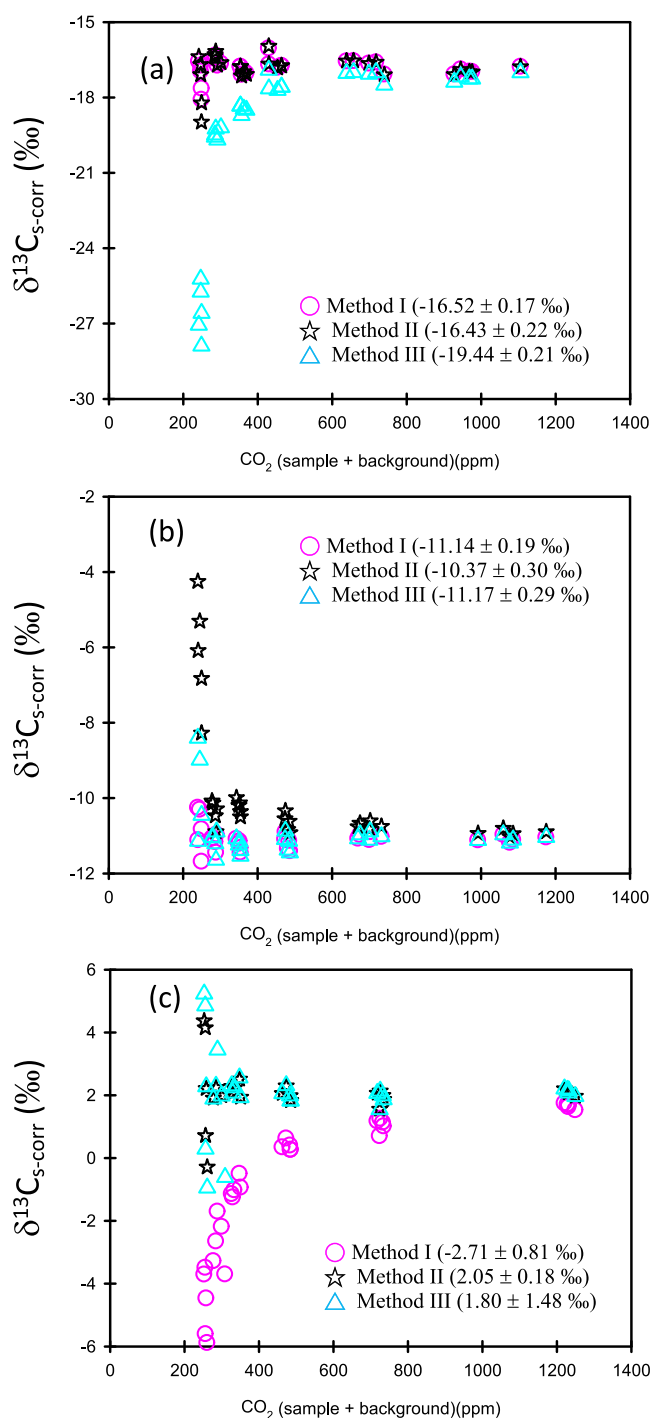


**Figure 3.** Scatter plots between corrected  $\delta^{13}\text{C}$  values and  $\text{CO}_2$  concentrations (sample + background) in (a) KHP, (b) sucrose A, and (c) sucrose B through different pairs of standards. The corrected method is described in the text.

standards when the  $\text{CO}_2$  concentrations were higher than 290 ppm (equal to  $\sim 5 \mu\text{gC} + 200 \text{ ppm}$  background  $\text{CO}_2$ ). On the other hand, the standard deviation of  $\delta^{13}\text{C}$  values in all working standards measured by method II was much more stable than those measured by method I and method II. This suggested that correction of  $\delta^{13}\text{C}$  by method II was more precise for the standard containing carbon content more than  $5 \mu\text{g}$ . Thus, we selected method II as an appropriate approach to calculate the corrected  $\delta^{13}\text{C}$  in standards and aerosol samples. Furthermore,

we attempted to calculate the uncertainty of the corrected  $\delta^{13}\text{C}$  values estimated by method II using error propagation.<sup>41</sup> The detailed calculation of this approach can be seen in the Supporting Information S3. Using method II, the corrected  $\delta^{13}\text{C}$  values of the three working standards with the different weights of carbon content are listed in Table 1. The uncertainty obtained by the error propagation is also listed (fourth column in Table 1). The results showed that the average  $\delta^{13}\text{C}$  values of KHP, sucrose A, and sucrose B (carbon content in each standard was higher than  $5 \mu\text{gC}$ ) were  $-16.72\text{‰}$ ,  $-10.57\text{‰}$ , and  $2.05\text{‰}$ , respectively. The uncertainty of corrected  $\delta^{13}\text{C}$  values in all working standards decreased with increasing carbon contents. The uncertainties of corrected  $\delta^{13}\text{C}$  values in KHP, sucrose A, and sucrose B were  $0.38\text{‰}$ ,  $0.48\text{‰}$ , and  $0.39\text{‰}$ , respectively, when the carbon contents were  $5 \mu\text{g}$ . This suggested that the absolute precision of the corrected  $\delta^{13}\text{C}$  was better than  $0.5\text{‰}$  for standards containing carbon content more than  $5 \mu\text{g}$ .

Using the Keeling approach, the corrected  $\delta^{13}\text{C}$  values ( $\delta^{13}\text{C}_{\text{s-corr}}$ ) of KHP, sucrose A, and sucrose B were  $-16.72\text{‰}$ ,  $-10.57\text{‰}$ , and  $2.05\text{‰}$ , respectively. Indeed, the reference  $\delta^{13}\text{C}$  values ( $\delta^{13}\text{C}_{\text{s-cali}}$ ) of KHP, sucrose A, and sucrose B calibrated by IRMS were  $-30.4$ ,  $-25.0$ , and  $-12.2\text{‰}$ , respectively. Obviously, a big difference between the corrected and reference  $\delta^{13}\text{C}$  values was found in each working standard. The primary reason for these differences was due to the fact that the CRDS instrument was internally calibrated using air as a carrier gas but operated using Ar as a carrier gas. Because of line-shape effects, the reported isotope ratio was affected by the composition, and the effect can be found in the literature studies.<sup>42–44</sup> Consequently, the  $\delta^{13}\text{C}_{\text{s-corr}}$  values needed to be calibrated using a linear regression between  $\delta^{13}\text{C}_{\text{s-corr}}$  and  $\delta^{13}\text{C}_{\text{s-cali}}$  values. Using the linear regression line, we can calculate the calibrated  $\delta^{13}\text{C}_{\text{s-cali}}$  as

$$\delta^{13}\text{C}_{\text{s-cali}} = a \times \delta^{13}\text{C}_{\text{s-corr}} + b \quad (11)$$

where  $a$  and  $b$  are the slope and intercept of this linear regression. As shown in Figure S7,  $a$  and  $b$  were  $0.99$  and  $-14.24$ , respectively, in this case. In terms of field online measurements of  $\delta^{13}\text{C}$  in carbonaceous aerosols, the same aforementioned procedure has to be carried out, and the linear regression line between  $\delta^{13}\text{C}_{\text{s-cali}}$  and  $\delta^{13}\text{C}_{\text{s-corr}}$  has to be obtained prior to field measurements. After that, we can continuously monitor  $\delta^{13}\text{C}$  values through this system, and the real  $\delta^{13}\text{C}$  values in atmospheric carbonaceous aerosols can be then corrected using eq 11.

**3.3. Comparisons with IR-MS Results.** To inspect the accuracy of  $\delta^{13}\text{C}$  in carbonaceous aerosols measured using the OC/EC analyzer-CRDS system, we further compared the  $\delta^{13}\text{C}$  values in TC ( $\delta^{13}\text{C}\text{-TC}$ ) determined by the new system and a traditional IRMS technique (IR-MS, MAT 253, Thermo Fisher Scientific, USA). To make this comparison, the aerosol samples collected in NUIST (see Section 2.2) were used to analyze the  $\delta^{13}\text{C}\text{-TC}$  using the OC/EC analyzer-CRDS system and IRMS. For the IRMS method, the punched quartz filters were combusted at  $850 \text{ }^\circ\text{C}$  in an elemental analyzer, in order to convert carbon content to  $\text{CO}_2$ . After conversion,  $\text{CO}_2$  was directly introduced into IRMS without any pretreatment, and the  $\delta^{13}\text{C}\text{-TC}$  was then determined. Figure S8 plots the  $\delta^{13}\text{C}\text{-TC}$  values measured using OC/EC analyzer-CRDS and IR-MS systems. As seen,  $\delta^{13}\text{C}\text{-TC}$  determined by the built system correlated well ( $R^2 = 0.89$ ,  $N = 7$ ) with that obtained by IRMS with a slope of  $0.998$ . Assuming that  $\delta^{13}\text{C}\text{-TC}$  measured using

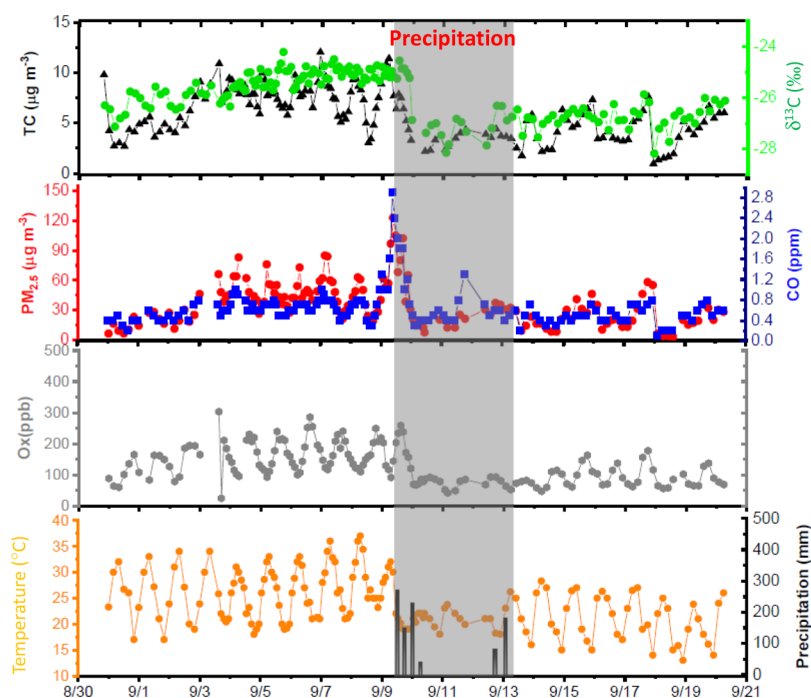


**Figure 4.** Time series of TC mass,  $\delta^{13}\text{C}$ -TC,  $\text{PM}_{2.5}$  mass, CO,  $\text{O}_3$ , ambient temperature, and precipitation in Beijing during the sampling period. Precipitation is 6 h accumulated rainfall. The gray shadow denotes the precipitation days.

the IRMS was a real  $\delta^{13}\text{C}$  value, we estimated that the error of  $\delta^{13}\text{C}$ -TC by our system was in a range of  $-0.18$  to  $0.21\text{‰}$ . On average, the  $\delta^{13}\text{C}$ -TC values measured using the OC/EC analyzer-CRDS system and IR-MS were  $-26.23 \pm 0.10\text{‰}$  (uncertainty was obtained by the error propagation) and  $-26.27 \pm 0.65\text{‰}$ , respectively, and the difference between the two systems was  $-0.04\text{‰}$ . This suggested that our method enables the determination of  $\delta^{13}\text{C}$ -TC of the atmospheric carbonaceous aerosols. Thus, we applied our developed system to continuously measure  $\delta^{13}\text{C}$ -TC in the atmospheric  $\text{PM}_{2.5}$  over Beijing from August 30 to September 20, 2019. In the next section, we will report the  $\delta^{13}\text{C}$  values and track potential sources and atmospheric processing of carbonaceous aerosols in Beijing.

**3.4. Application in  $\delta^{13}\text{C}$ -TC Measurements over Beijing.** **3.4.1. Characteristics of  $\delta^{13}\text{C}$ -TC.** We employed this system to monitor  $\delta^{13}\text{C}$ -TC values in  $\text{PM}_{2.5}$  in Beijing from August 30 to September 20, 2019. During the sampling period, the OC/EC analyzer-CRDS system was installed at a monitoring station, which is located on the rooftop of a two-story building in China National Environmental Monitoring Centre (CNEMC). CNEMC is encompassed by the traffic roads, indicating that traffic emission might be an important source of atmospheric carbonaceous aerosols. To obtain the accurate and precise  $\delta^{13}\text{C}$  data, the carbon content in aerosol samples for the OC/EC analyzer-CRDS system had to exceed  $5 \mu\text{g}$  (see Section 3.2). During the sampling period, the TC concentrations varied from  $1.0$  to  $12.0 \mu\text{g m}^{-3}$  (Figure 4). This indicated that the carbon content in each aerosol sample was from  $0.48$  to  $5.8 \mu\text{g}$  (for 1 h time resolution sampling with a flow rate of  $45 \text{ mL min}^{-1}$ ), which was not enough for determination of  $\delta^{13}\text{C}$  in some low-carbon content samples. Thus, we extended the sampling duration time to 2–4 h, and 97% samples possessed a carbon content of higher than  $5 \mu\text{g}$ , which was a minimum required carbon content for  $\delta^{13}\text{C}$  analysis in the developed system. Figure 4 plots time series of

the  $\delta^{13}\text{C}$ -TC values with a time resolution of 2–4 h in Beijing during the sampling period. The data of other air pollutants, such as  $\text{PM}_{2.5}$ ,  $\text{O}_3$ ,  $\text{NO}_2$ , and CO, were also obtained from the Olympic Sports Center air quality monitoring station, which is situated in the south direction of CNEMC with a distance of approximately 4 km. The weather parameters, such as temperature and precipitation, were also acquired from Capital International Airport located in the east direction of the receptor site with a distance of 16 km. The  $\delta^{13}\text{C}$ -TC varied from  $-28.2$  to  $-24.2\text{‰}$  and averaged at  $-25.9 \pm 0.9\text{‰}$  without any significant diurnal patterns (Figure S9a). On the other hand, our  $\delta^{13}\text{C}$ -TC value was in agreement with those observed in other megacities over China (see in Figure S9b), where carbonaceous aerosols were strongly influenced by gasoline and diesel vehicles in summer.<sup>18</sup>

Based on  $^{14}\text{C}$  measurements, both fossil fuel and nonfossil fuel emissions (e.g., BB, vegetation emissions, and cooking) were major sources of particulate TC in Beijing during summer season.<sup>10</sup> In this work, our  $\delta^{13}\text{C}$ -TC values varied from  $-28.2$  to  $-24.2\text{‰}$ , which fell into the range of liquid fuels and  $\text{C}_3$  plants (see in Figure S9c). This implied that liquid fuel and primary and secondary  $\text{C}_3$  plants were likely the dominant sources of TC in Beijing during the hot season.

**3.4.2. Influence of Heavy Precipitation on  $\delta^{13}\text{C}$ -TC.** Apart from tracking sources,  $\delta^{13}\text{C}$  can also provide a hint for understanding atmospheric processing of carbonaceous aerosols.<sup>14,24,28</sup> During the Beijing campaign, heavy precipitation events occurred at noontime on September 9 and the event lasted for 3 days, in which a maxima of 6 h-accumulated precipitation reached 270 mm. As shown in Figure 4, the concentrations of  $\text{PM}_{2.5}$  mass (TC) decreased from  $174$  to  $34 \mu\text{g m}^{-3}$  ( $10$  to  $3 \mu\text{g m}^{-3}$ ) after half a day of precipitation. This suggested that precipitation likely washed out most of the aerosols from the polluted atmosphere. Interestingly, we also found a large depletion of  $\delta^{13}\text{C}$  values after the heavy precipitation event. Assuming the changes in emissions from

combustion of liquid fuels and C<sub>3</sub> plants before and after the precipitation were insignificant, the higher  $\delta^{13}\text{C}$  values before precipitation might be explained by the photochemical aging process.<sup>14,29</sup> Here, we used O<sub>x</sub> (O<sub>x</sub> = NO<sub>2</sub> + O<sub>3</sub>) concentration as an index of atmospheric photo-oxidation. As illustrated in Figure 4, the daily O<sub>x</sub> maximum concentration (regularly at 2 p.m.) was 228 ± 53 ppb before the precipitation events, which was 2.6 times higher than that (87 ± 5 ppb) during the precipitation days (on September 10, 11, and 12). This indicated that photochemical capacity before heavy precipitation was much stronger than that during precipitation. During the heavy precipitation events, aged aerosols have been washed out from the atmosphere and resulted in significant decreases in TC concentrations. Instead, relative fresh aerosols from various sources emitted into the atmosphere. Consequently, the weak-photochemical and fresh aerosols might explain the depleted  $\delta^{13}\text{C}$ -TC values during precipitation. On the other hand, the average  $\delta^{13}\text{C}$ -TC value on September 9 was -25.0‰ (before the precipitation event), which was higher than that (-27.4‰) on September 10 (during the precipitation event). This suggested that the heavy rainfall decreased  $\delta^{13}\text{C}$ -TC by approximately 2.4‰. After September 13, the temperature and the daily maximum O<sub>x</sub> concentration gradually increased, reflecting that the photochemical capacity was getting stronger day by day. Interestingly, the  $\delta^{13}\text{C}$  increased with TC concentrations because a significant positive correlation ( $R = 0.76$  and  $p < 0.05$ , Figure S10) between  $\delta^{13}\text{C}$ -TC and TC was found after precipitation events. This might suggest that the atmospheric photochemical aging process increased TC concentrations, resulting in enrichment of  $\delta^{13}\text{C}$  values.

#### 4. CONCLUSIONS

In this work, a novel system for synchronously monitoring concentrations of TC and its accompanying  $\delta^{13}\text{C}$  values was developed by combining a Sunset OC/EC analyzer and a Picarro CRDS system. The accuracy was better than 0.1‰, and the absolute precision was less than 0.5‰ for the sample containing a carbon content of higher than 5 μg. We further employed this system to measure  $\delta^{13}\text{C}$ -TC in Beijing during the late summer and early autumn of 2019 with a time resolution of 2–4 h. The results showed that  $\delta^{13}\text{C}$ -TC varied from -28.2‰ to -24.2‰ (mean value was  $-25.9 \pm 0.9\%$ ) without significant diurnal variations. Compared with the  $\delta^{13}\text{C}$  signatures from various emission sources, we found that liquid fuel and primary and secondary C<sub>3</sub> plants were likely the dominant sources of TC in Beijing during the sampling period.

Source apportionments and atmospheric processing of carbonaceous aerosols are important issues regarding atmospheric research. In this study, the OC/EC analyzer-CRDS system enables to determine  $\delta^{13}\text{C}$ -TC with high accuracy and precision and high-time resolution. Limited to the weights of carbon content, we could not measure the carbon isotopic compositions of OC and EC with high-time resolution. Previous numerous studies have focused on  $\delta^{13}\text{C}$  values in OC and EC aerosols.<sup>10,14</sup> Unfortunately, these studies only provided  $\delta^{13}\text{C}$  in OC and EC aerosols with poor time resolution (at least a half-day sampling). This cannot provide better understanding of the temporal evolution of source apportionments and atmospheric processes of particulate OC and EC. Thus, establishment of the online measurements of  $\delta^{13}\text{C}$  in OC and EC aerosols is needed, leading to better

understanding of the temporal behaviors and potential sources of carbonaceous aerosols on short-time scales in the future.

#### ■ ASSOCIATED CONTENT

##### Supporting Information

The Supporting Information is available free of charge at <https://pubs.acs.org/doi/10.1021/acs.analchem.0c02063>.

NIOSH 5040 thermal–optical protocol used in analysis of OC/EC in NUIST aerosol samples; temperature in the oven and produced CO<sub>2</sub> concentrations; scatter plots; long-term stability of  $\delta^{13}\text{C}$  measured by CRDS and distributions in numbers of counts of individual  $\delta^{13}\text{C}$  values; and  $\delta^{13}\text{C}$  values in carbonaceous aerosols (PDF)

#### ■ AUTHOR INFORMATION

##### Corresponding Author

**Yan-Lin Zhang** – Yale-NUIST Center on Atmospheric Environment, International Joint Laboratory on Climate and Environment Change and Key Laboratory Meteorological Disaster; Ministry of Education & Collaborative Innovation Center on Forecast and Evaluation of Meteorological Disaster, Nanjing University of Information Science and Technology, Nanjing 210044, China; Jiangsu Provincial Key Laboratory of Agricultural Meteorology, School of Applied Meteorology, Nanjing University of Information Science & Technology, Nanjing 210044, China; [orcid.org/0000-0002-8722-8635](https://orcid.org/0000-0002-8722-8635); Email: [dryanlinzhang@outlook.com](mailto:dryanlinzhang@outlook.com), [zhangyanlin@nuist.edu.cn](mailto:zhangyanlin@nuist.edu.cn)

##### Authors

**Yu-Chi Lin** – Yale-NUIST Center on Atmospheric Environment, International Joint Laboratory on Climate and Environment Change and Key Laboratory Meteorological Disaster; Ministry of Education & Collaborative Innovation Center on Forecast and Evaluation of Meteorological Disaster, Nanjing University of Information Science and Technology, Nanjing 210044, China; Jiangsu Provincial Key Laboratory of Agricultural Meteorology, School of Applied Meteorology, Nanjing University of Information Science & Technology, Nanjing 210044, China; [orcid.org/0000-0003-4227-8978](https://orcid.org/0000-0003-4227-8978)

**Feng Xie** – Yale-NUIST Center on Atmospheric Environment, International Joint Laboratory on Climate and Environment Change and Key Laboratory Meteorological Disaster; Ministry of Education & Collaborative Innovation Center on Forecast and Evaluation of Meteorological Disaster, Nanjing University of Information Science and Technology, Nanjing 210044, China; Jiangsu Provincial Key Laboratory of Agricultural Meteorology, School of Applied Meteorology, Nanjing University of Information Science & Technology, Nanjing 210044, China

**Wen-Qi Zhang** – Yale-NUIST Center on Atmospheric Environment, International Joint Laboratory on Climate and Environment Change and Key Laboratory Meteorological Disaster; Ministry of Education & Collaborative Innovation Center on Forecast and Evaluation of Meteorological Disaster, Nanjing University of Information Science and Technology, Nanjing 210044, China; Jiangsu Provincial Key Laboratory of Agricultural Meteorology, School of Applied Meteorology, Nanjing University of Information Science & Technology, Nanjing 210044, China

**Mei-Yi Fan** – Yale-NUIST Center on Atmospheric Environment, International Joint Laboratory on Climate and Environment

Change and Key Laboratory Meteorological Disaster; Ministry of Education & Collaborative Innovation Center on Forecast and Evaluation of Meteorological Disaster, Nanjing University of Information Science and Technology, Nanjing 210044, China; Jiangsu Provincial Key Laboratory of Agricultural Meteorology, School of Applied Meteorology, Nanjing University of Information Science & Technology, Nanjing 210044, China; [orcid.org/0000-0002-3311-8799](https://orcid.org/0000-0002-3311-8799)

Zhiwei Lin – Picarro Inc., Santa Clara, California 95054, United States

Chris W. Rella – Picarro Inc., Santa Clara, California 95054, United States

John A. Hoffnagle – Picarro Inc., Santa Clara, California 95054, United States

Complete contact information is available at:

<https://pubs.acs.org/10.1021/acs.analchem.0c02063>

## Notes

The authors declare no competing financial interest.

## ACKNOWLEDGMENTS

This study was financially supported by the National Key R&D Program of China (Grant no. 2017YFC0212700), the Natural Scientific Foundation of China (no. 41977305), the Provincial Natural Science Foundation of Jiangsu (no. BK20180040), and Jiangsu Innovation & Entrepreneurship Team. We would like to thank the Sunset Laboratory Inc. and China National Environmental Monitoring Centre for the assistance in development of the monitoring system and field measurement.

## REFERENCES

- (1) Jimenez, J. L.; Canagaratna, M. R.; Donahue, N. M.; Prevot, A. S. H.; Zhang, Q.; Kroll, J. H.; Decarlo, P. F.; Allan, J. D.; Coe, H.; Ng, N. L.; Aiken, A. C.; Docherty, K. S.; Ulbrich, I. M.; Grieshop, A. P.; Robinson, A. L.; Duplissy, J.; Smith, J. D.; Wilson, K. R.; Lanz, V. A.; Hueglin, C.; Sun, Y. L.; Tian, J.; Laaksonen, A.; Raatikainen, T.; Rautiainen, J.; Vaattovaara, P.; Ehn, M.; Kulmala, M.; Tomlinson, J. M.; Collins, D. R.; Cubison, M. J.; Dunlea, J.; Huffman, J. A.; Onasch, T. B.; Alfarra, M. R.; Williams, P. I.; Bower, K.; Kondo, Y.; Schneider, J.; Drewnick, F.; Borrmann, S.; Weimer, S.; Demerjian, K.; Salcedo, D.; Cottrell, L.; Griffin, R.; Griffin, A.; Miyoshi, T.; Hatakeyama, S.; Shimono, A.; Sun, J. Y.; Zhang, Y. M.; Dzepina, K.; Kimmel, J. R.; Sueper, D.; Jayne, J. T.; Herndon, S. C.; Trimborn, A. M.; Williams, L. R.; Wood, E. C.; Middlebrook, A. M.; Kolb, C. E.; Baltensperger, U.; Worsnop, D. R. *Science* **2009**, *326*, 1525–1529.
- (2) Chou, C. C.-K.; Lee, C. T.; Cheng, M. T.; Yuan, C. S.; Chen, S. J.; Wu, Y. L.; Hsu, W. C.; Lung, S. C.; Hsu, S. C.; Lin, C. Y.; Liu, S. C. *Atmos. Chem. Phys.* **2010**, *10*, 9563–9578.
- (3) Huang, R.-J.; Zhang, Y.; Bozzetti, C.; Ho, K.-F.; Cao, J.-J.; Han, Y.; Daellenbach, K. R.; Slowik, J. G.; Platt, S. M.; Canonaco, F.; Zotter, P.; Wolf, R.; Pieber, S. M.; Bruns, E. A.; Crippa, M.; Ciarelli, G.; Piazzalunga, A.; Schwikowski, M.; Abbazade, G.; Schnelle-Kreis, J.; Zimmermann, R.; An, Z.; Szidat, S.; Baltensperger, U.; Haddad, I. E.; Prévôt, A. S. H. *Nature* **2014**, *514*, 218–222.
- (4) Zhao, B.; Wang, P.; Ma, J. Z.; Zhu, S.; Pozzer, A.; Li, W. *Atmos. Chem. Phys.* **2012**, *12*, 481–501.
- (5) Andrews, T.; Forster, P. M.; Boucher, O.; Bellouin, N.; Jones, A. *Geophys. Res. Lett.* **2010**, *37*, a.
- (6) Koch, D.; Del Genio, A. D. *Atmos. Chem. Phys.* **2010**, *10*, 7685–7696.
- (7) Ban-Weiss, G. A.; Cao, L.; Bala, G.; Caldeira, K. *Clim. Dynam.* **2012**, *38*, 897–911.
- (8) Wang, Q. Q.; Huang, X. H. H.; Zhang, T.; Zhang, Q.; Feng, Y.; Yuan, Z.; Wu, D.; Lau, A. K. H.; Yu, J. Z. *Atmos. Environ.* **2015**, *118*, 164–175.
- (9) Cao, F.; Zhang, Y.; Ren, L.; Liu, J.; Li, J.; Zhang, G.; Liu, D.; Sun, Y.; Wang, Z.; Shi, Z.; Fu, P. *Natl. Sci. Rev.* **2017**, *4*, 804–806.
- (10) Zhang, Y.; Ren, H.; Sun, Y.; Cao, F.; Chang, Y.; Liu, S.; Lee, X.; Agrios, K.; Kawamura, K.; Liu, D.; Ren, L.; Du, W.; Wang, Z.; Prévôt, A. S. H.; Szidat, S.; Fu, P. *Environ. Sci. Technol.* **2017**, *51*, 7842–7852.
- (11) Bian, Q.; Alharbi, B.; Shareef, M. M.; Husain, T.; Pasha, J. M.; Atwood, S. A.; Kriedenweiss, S. M. *Atmos. Chem. Phys. Atmos. Chem. Phys.* **2018**, *18*, 3969–3985.
- (12) Briggs, N. L.; Long, C. M. *Atmos. Environ.* **2016**, *144*, 409–427.
- (13) Salma, I.; Németh, Z.; Weidinger, T.; Maenhaut, W.; Claeys, M.; Molnár, M.; Major, I.; Ajtai, T.; Utry, N.; Bozók, Z. *Atmos. Chem. Phys.* **2017**, *17*, 13767–13781.
- (14) Zhang, W.; Zhang, Y.-L.; Cao, F.; Xiang, Y.; Zhang, Y.; Bao, M.; Liu, X.; Lin, Y.-C. *Atmos. Chem. Phys.* **2019**, *19*, 11071–11087.
- (15) Widory, D.; Roy, S.; Le Moullec, Y.; Goupil, G.; Cocherie, A.; Guerrot, C. *Atmos. Environ.* **2004**, *38*, 953–961.
- (16) Kawashima, H.; Haneishi, Y. *Atmos. Environ.* **2012**, *46*, 568–579.
- (17) Andersson, A.; Deng, J.; Du, K.; Zheng, M.; Yan, C.; Sköld, M.; Gustafsson, Ö. *Environ. Sci. Technol.* **2015**, *49*, 2038–2043.
- (18) Cao, J.-J.; Chow, J. C.; Tao, J.; Lee, S.-C.; Watson, J. G.; Ho, K.-F.; Wang, G.-H.; Zhu, C.-S.; Han, Y.-M. *Atmos. Environ.* **2011**, *45*, 1359–1363.
- (19) Kohn, M. J. *Proc. Natl. Acad. Sci. U.S.A.* **2010**, *107*, 19691–19695.
- (20) Kawashima, H.; Haneishi, Y. *Atmos. Environ.* **2012**, *46*, 568–579.
- (21) Das, O.; Wang, Y.; Hsieh, Y.-P. *Org. Geochem.* **2010**, *41*, 263–269.
- (22) Martinsson, J.; Andersson, A.; Sporre, M. K.; Friberg, J.; Kristensson, A.; Swietlicki, E.; Olsson, P.-A.; Stenström, K. E. *Aerosol Air Qual. Res.* **2017**, *17*, 2081–2094.
- (23) Bosch, C.; Andersson, A.; Kirillova, E. N.; Budhavant, K.; Tiwari, S.; Praveen, P.; Russell, L. M.; Beres, N. D.; Ramanatham, V.; Gustafsson, Ö. *J. Geophys. Res. Atmos.* **2014**, *119*, 11743–11759.
- (24) Kirillova, E. N.; Andersson, A.; Sheesley, R. J.; KrusÅ, M.; Praveen, P. S.; Budhavant, K.; Safai, P. D.; Rao, P. S. P.; Gustafsson, Ö. *J. Geophys. Res. Atmos.* **2013**, *118*, 614–626.
- (25) Masalait, A.; Holzinger, R.; Remeikis, V.; Röckmann, T.; Dusek, U. *Atmos. Environ.* **2017**, *148*, 62–76.
- (26) Zhao, Z.; Cao, J.; Zhang, T.; Shen, Z.; Ni, H.; Tian, J.; Wang, Q.; Liu, S.; Zhou, J.; Gu, J.; Shen, G. *Atmos. Environ.* **2018**, *185*, 253–261.
- (27) Ni, H.; Huang, R.-J.; Cao, J.; Liu, W.; Zhang, T.; Wang, M.; Meijer, H. A. J.; Dusek, U. *Atmos. Chem. Phys.* **2018**, *18*, 16363–16383.
- (28) Rudolph, J.; Anderson, R. S.; Czapiewski, K. V.; Czuba, E.; Ernst, D.; Gillespie, T.; Huang, L.; Rigby, C.; Thompson, A. E. *J. Atmos. Chem.* **2003**, *44*, 39–55.
- (29) Bikina, S.; Andersson, A.; Ram, K.; Sarin, M. M.; Sheesley, R. J.; Kirillova, E. N.; Rengarajan, R.; Sudheer, A. K.; Gustafsson, Ö. *J. Geophys. Res. Atmos.* **2017**, *122*, 4903–4923.
- (30) Zhang, Y.-L.; Kawamura, K.; Cao, F.; Lee, M. *J. Geophys. Res. Atmos.* **2016**, *121*, 3707–3717.
- (31) Vodička, P.; Kawamura, K.; Schwarz, J.; Kunwar, B.; Ždimal, V. *Atmos. Chem. Phys.* **2019**, *19*, 3463–3479.
- (32) Vogel, F. R.; Huang, L.; Ernst, D.; Giroux, L.; Racki, S.; Worthy, D. E. *J. Atmos. Meas. Tech.* **2013**, *6*, 301–308.
- (33) Yu, X.-Y.; Cary, R. A.; Laulainen, N. S. *Atmos. Chem. Phys.* **2009**, *9*, 6793.
- (34) Dao, X.; Lin, Y.-C.; Cao, F.; Di, S.-Y.; Hunag, Y.; Xin, G.; Li, J.; Fu, P.; Zhang, Y.-L. *Bull. Am. Meteorol. Soc.* **2019**, *101*, ES337–ES351.
- (35) Berryman, E. M.; Marshall, J. D.; Rahn, T.; Cook, S. P.; Litvak, M. *Rapid Commun. Mass Spectrom.* **2011**, *25*, 2355–2360.
- (36) Birch, M. E.; Cary, R. A. *Aerosol Sci. Technol.* **1996**, *25*, 221–241.
- (37) Malowany, K.; Stix, J.; Van Pelt, A.; Lucic, G. *Atmos. Meas. Tech.* **2015**, *8*, 4075.

- (38) Pataki, D. Z.; Zhleringer, J. R.; Flanagan, L. B.; Yakir, D.; Bowling, D. R.; Still, C. J.; Buchmann, N.; Kaplan, J. O.; Berry, J. A. *Global Biogeochem. Cycles* **2003**, *17*, 1022.
- (39) Kaul, D. S.; Ning, Z.; Westerdahl, D.; Yin, X.; Cay, R. A. *Aerosol Air Qual. Res.* **2016**, *16*, 1345–1355.
- (40) Schnyder, H.; Schäufole, R.; Wenzel, R. *Rapid Commun. Mass Spectrom.* **2004**, *18*, 3068–3074.
- (41) Polissar, P. J.; Fulton, J. M.; Junium, C. K.; Turich, C. C.; Freeman, K. H. *Anal. Chem.* **2009**, *81*, 755–763.
- (42) Friderichs, G.; Bock, J.; Temps, F.; Fietzek, P.; Körtzinger, A.; Wallace, D. W. R. *Limnol. Oceanogr.: Methods* **2010**, *8*, 539–551.
- (43) Rella, C.; Hoffnagle, J.; He, Y.; Tajima, S. *Atmos. Meas. Tech.* **2015**, *8*, 4539–4559.
- (44) Johnson, J. E.; Rella, C. W. *Atmos. Meas. Tech.* **2017**, *10*, 3073–3091.